Rheological Properties of Metallocene Isotactic Polypropylenes

MITSUYOSHI FUJIYAMA, HITOSHI INATA

Tokuyama Research Laboratory, Tokuyama Corp., 1-1, Harumi-cho, Tokuyama-shi, Yamaguchi-ken, 745-0024 Japan

Received 11 June 2001; accepted 6 September 2001

ABSTRACT: Rheological properties of metallocene-catalyzed isotactic polypropylenes (MET-PP) were evaluated in comparison with those of Ziegler–Natta-catalyzed isotactic polypropylenes (ZN-PP) and MET-PP was generally characterized in a rheological aspect. Based on the characterization, various flow processibilities and their effect on the higher order structure and product properties of the processed article were estimated. The capillary flow properties at various temperatures, elongational flow properties, and dynamic viscoelasticities of MET-PPs and ZN-PPs with various melt flow indexes (MFIs) were measured. Furthermore, as an example of application of rheological analysis, the selection of proper raw resin and processing conditions in the sheet-extrusion of MET-PP was studied. MET-PP shows the following rheological features due mainly to the narrow molecular weight distribution in comparison with ZN-PP with equivalent MFI to that of MET-PP: while the viscosities at low shear rates are lower, those at high shear rates are higher. Although there is little difference in the loss modulus G'' (viscosity), the storage modulus G' (elasticity) is very (about one decade) lower. The die swell is much smaller. The entrance pressure loss and end correction coefficient are lower. The critical shear rate at which a melt fracture begins to occur is lower. The melt tension, elongational viscosity, and melt flow index ratio are lower. The flow activation energy is slightly lower. The zero-shear viscosity obeys the 3.4th-power law independent of catalyst. © 2002 Wiley Periodicals, Inc. J Appl Polym Sci 84: 2157–2170, 2002

Key words: isotactic polypropylene; metallocene catalyst; Ziegler–Natta catalyst; rheology; processing

INTRODUCTION

In 1980, Sinn and Kaminsky[1,2] presented a homogeneous metallocene catalyst which is composed of a metallocene complex and methylalumoxane (MAO) and is very active to ethylene polymerization. The metallocene catalyst was actively studied worldwide since its discovery and the commercial production of linear low-density polyethylene (LLDPE) by use of the catalyst was begun first in 1991, followed by the commercial production of syndiotactic polypropylene in 1993 and of isotactic polypropylene (PP) in 1995.

Because the active site of metallocene catalyst is single, PP [metallocene-catalyzed isotactic polypropylene (MET-PP)] polymerized by use of the catalyst has a feature of narrow distribution of molecular weight, crystallinity, and composition and of little low molecular weight component. Furthermore, from the viewpoint of polymerization mechanism of the catalyst, it contains much

Correspondence to: M. Fujiyama (m-fujiyama@tokuyama.co.jp).

Journal of Applied Polymer Science, Vol. 84, 2157–2170 (2002)

Table I Characteristics of Samples

Term	Metallocene PP				Ziegler-Natta PP		
	MET-1	MET-2	MET-3	MET-4	ZN-1	ZN-2	ZN-3
M_w ($\times 10^5$)	3.75	3.29	2.05	2.10	4.34	4.16	2.33
M_n ($\times 10^4$)	15.0	13.7	10.3	9.5	7.2	6.7	4.1
M_w/M_n	2.5	2.4	2.0	2.2	6.0	6.2	5.7
p-Xylene extraction (wt %)	0.3	0.2	0.1	0.4	2.0	5.5	1.9
T_m (°C)	147	146	150	149	159	145	162
MFI (g/10 min)	1.66	2.16	6.3	8.2	2.12	2.39	8.5
MFIR	8.3	8.5	7.3	8.1	12.4	12.0	10.8
Die swell ratio	1.10	1.09	1.05	1.04	1.26	1.23	1.28

regioirregular bonds and shows a low melting point for high tacticity. The largest characteristic among molecular structures of MET-PP is the narrow molecular weight distribution and M_w/M_n of MET-PP is about 2 in comparison with 5–7 of Ziegler–Natta PP (ZN-PP). The narrow molecular weight distribution of MET-PP strongly influences its melt processibilities through the rheological properties and governs the resultant higher order structure and product properties.

In the present study, the rheological properties of MET-PPs were evaluated in comparison with those of ZN-PPs, and MET-PP was generally characterized in a rheological aspect. Based on the characterization, various flow processibilities and their effect on the higher order structure and product properties of processed article were estimated. Concretely, the capillary flow properties at various temperatures, elongational flow properties, and dynamic viscoelasticities of MET-PPs and ZN-PPs with various melt flow indexes (MFIs) were measured. Furthermore, as an example of application of rheological analysis, study on the selection of proper raw resin and processing conditions in the sheet-extrusion of MET-PP is reported.

EXPERIMENTAL

Samples

Table I shows the characteristics of samples. MET-PPs were prepared by use of an MAO-supported MET-PP catalyst and have narrow molecular weight distributions of M_w/M_n = 2–2.5. On

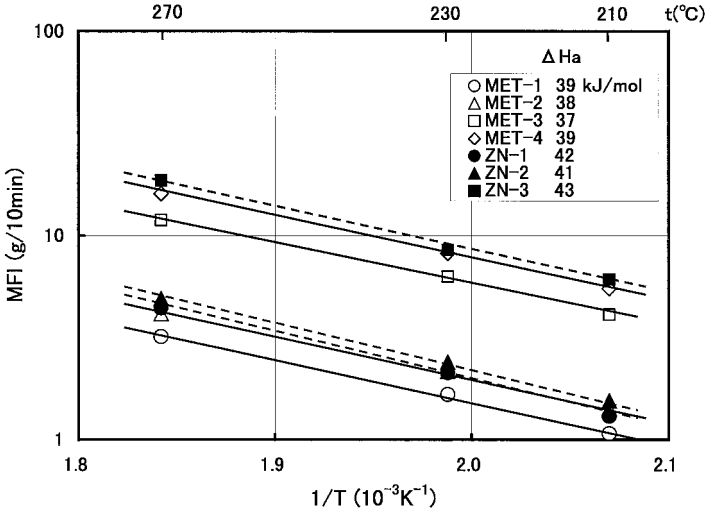

Figure 1 Temperature changes of MFI (Arrhenius plots).

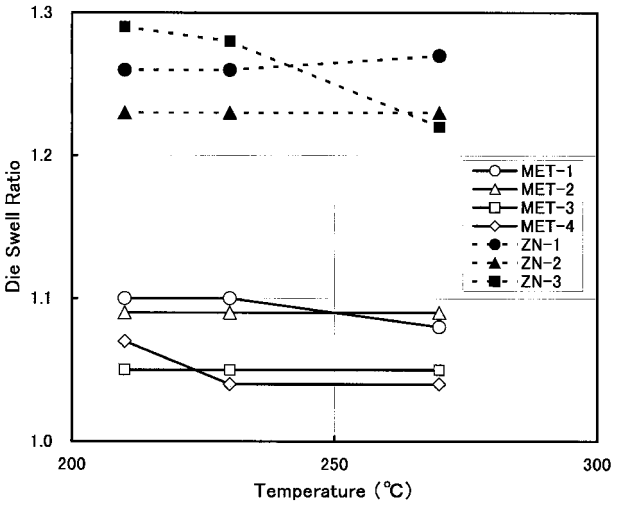

Figure 2 Temperature changes of die–swell ratio.

the other hand, ZN-PPs were prepared by use of an $MgCl_2$-supported titanium catalyst and have an M_w/M_n of about 6. ZN-1 and ZN-2 are random PP copolymers with ethylene contents of 0.5 and 3.7 wt %, respectively. Other samples are homo-PPs. MET-PPs also have characteristics of low *p*-xylene extraction (low molecular weight component) contents and low melting points. The melt flow index ratio (MFIR) and die–swell ratio are referred to in the Experimental Results section.

Measurements of Rheological Properties

Capillary Flow Properties

MFI and die swell ratio were measured with a melt indexer X416 type (Takara Thermistor Instruments Co. Ltd., Japan) under 2160 g load at 210, 230, and 270°C. As a measure of non-Newtonianity of flow, MFIR (the ratio of MFI under a load of 2160 g to that under a load of 325 g) was measured at 230°C.

Capillary flow properties were measured with a capillary rheometer Capirograph 1B type (Toyo Measurement Instruments Co. Ltd., Japan). The flow curve, die–swell ratio, and melt fracture behaviors were measured at 190, 230, and 270°C by use of a die with a capillary length L of 10 mm and a capillary diameter D of 1 mm. The end correction coefficient ν and entrance pressure loss P_0 were measured at 270°C by use of dies with a diameter D of 1 mm and lengths L of 20, 10, and 5 mm. The entrance pressure loss P_0 is the pressure loss by contraction of flow at the capillary entrance and the end correction coefficient ν is its nondimensional measure. The change of elongational viscosity λ with elongational strain rate $\dot{\epsilon}$ was calculated from P_0 according to the Cogswell's method.[3]

Melt Tension

Melt tension was measured with a Capirograph by use of a die with L of 20 mm and D of 2 mm under an extrusion speed of 5 mm/min and a take-off speed of 10 m/min at 270°C.

Dynamic Viscoelasticity

The storage modulus $G'(\omega)$, loss modulus $G''(\omega)$, dynamic viscosity $\eta'(\omega)$, and absolute value of complex viscosity $|\eta^*|(\omega)$ were measured at 270°C under N_2 atmosphere with a concentric cylinder rheometer (Rheometer Almighty, Iwamoto Seisakusho Co., Ltd., Japan). $|\eta^*|(\omega)$ was measured at 210°C and the zero-shear viscosity η_0 was obtained from $|\eta^*|(\omega)$ at low ω.

Sheet Extrusion

Sheets measuring 1 mm thick and 250 mm wide were extruded with a 90-mm ϕ single-screw extruder EA-9 type (Modern Machinery Co., Ltd., Japan) equipped with a 310-mm-wide T-die of a lip clearance of 1.5 mm under resin temperatures of 270 and 230°C, an extrusion speed of 80 kg/h, and a haul-off speed of 6.6 m/min and the state of extrusion was observed.

RESULTS AND DISCUSSION

MFI, Die Swell, and MFIR

Figure 1 shows the temperature changes of MFI (Arrhenius plots). The flow activation energies

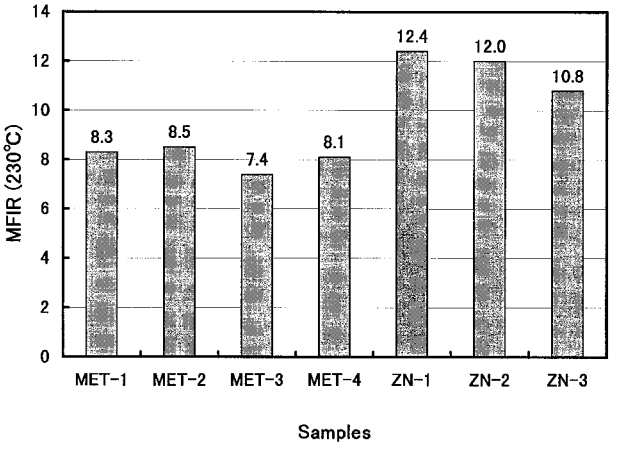

Figure 3 Comparison of MFIR among samples.

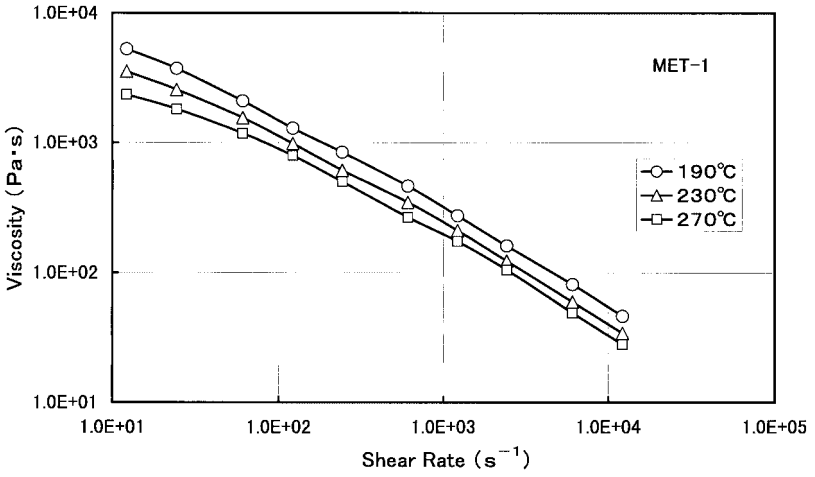

Figure 4 Flow curves of MET-1 sample at various temperatures.

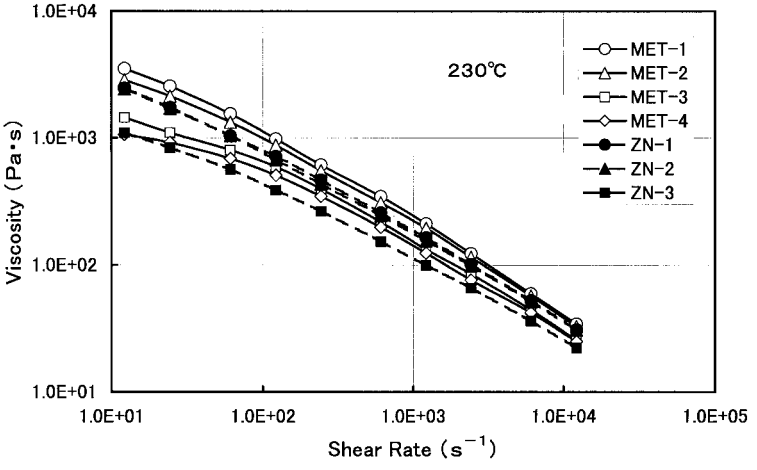

Figure 5 Comparison of flow curve among samples at 230°C.

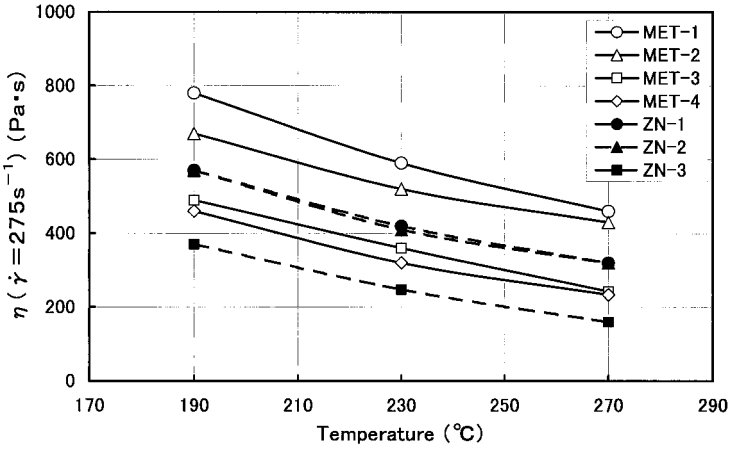

Figure 6 Comparison of temperature change of viscosity at sheet extrusion η ($\dot{\gamma}$ = 275 s^{-1}) among samples.

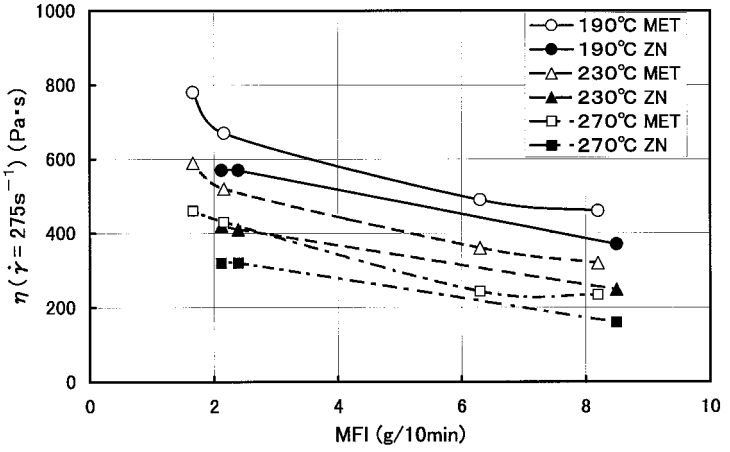

Figure 7 Dependence of viscosity at sheet extrusion η ($\dot{\gamma}$ = 275 s^{-1}) on MFI.

ΔHa obtained from the slope of lines are shown in the figure. ΔHa's of MET-PPs are 37–39 kJ/mol and are lower than those of ZN-PPs (41–43 kJ/mol) by about 10%.

Figure 2 shows the temperature changes of die–swell ratio at MFI measurement. MET-PPs show much lower die–swell ratios than ZN-PPs. This originates from the narrow molecular weight distribution and weak elasticity. Therefore, from this viewpoint, MET-PPs are suitable to profile extrusion in which high dimensional accuracy is needed. However, because MET-PPs show low viscosities at low shear rates, as shown later, they easily cause drawdown and their MFIs must be set considerably low for profile extrusion use.

Figure 3 shows the comparison of MFIR among samples. Because MET-PPs have narrow molecular weight distributions, they show very low MFIR of about 8 which is near 6.6 of Newtonian flow in comparison with 11–12 of ZN-PPs. A resin with low MFIR is superior in melt extensibility at spinning or film extrusion and is assumed to be able to be spun or extruded at high speed without draw resonance. It is assumed to be particularly suitable to extrusion lamination. Actually, Cheng and Kuo[4] show that an MET-PP can be cast by T-die without draw resonance up to a haul-off speed 17% higher than that of a ZN-PP with an equivalent MFI to that of the MET-PP.

Viscosity (Flow Curve)

Figure 4 exemplifies flow curves at various temperatures for a MET-1 sample and Figure 5 shows

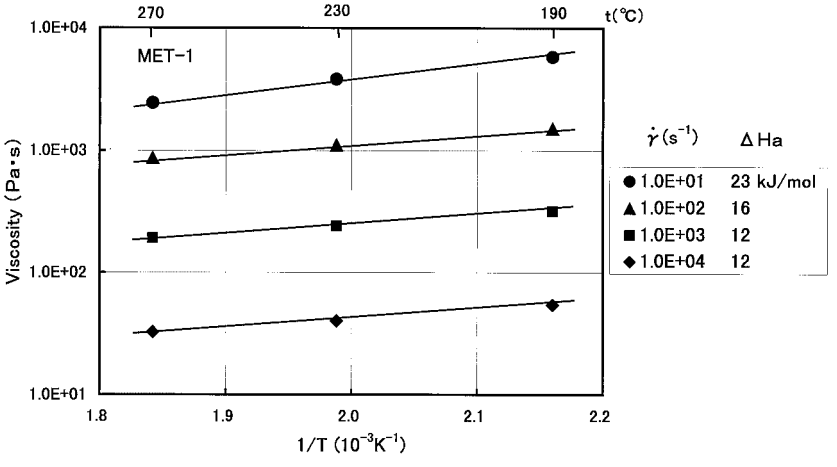

Figure 8 Temperature changes of MET-1 sample at various shear rates (Arrhenius plots).

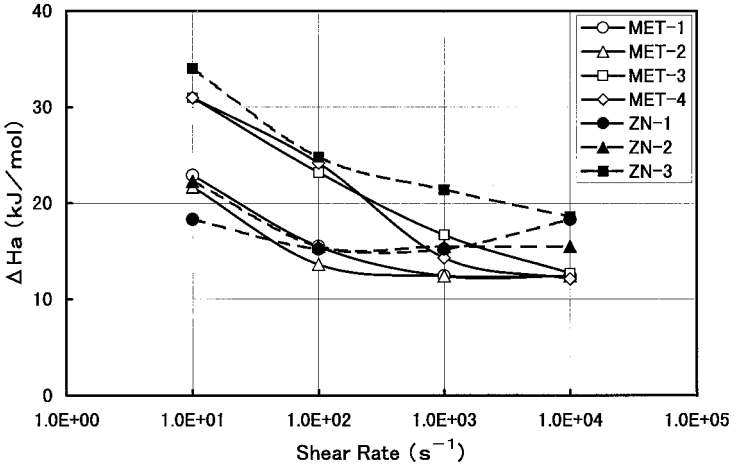

Figure 9 Changes of flow activation energy ΔHa with shear rate.

flow curves of various samples at 230°C as an example. Compared at an equivalent MFI, MET-PPs show higher viscosities, easier slopes of the flow curves, and weaker non-Newtonianities than ZN-PPs. Cheng and Kuo[4] have already reported that an MET-PP shows a smaller structural viscosity exponent and a weaker non-Newtonianity than a ZN-PP compared at the equivalent MFI as in the present experiment.

Figure 6 shows the changes of temperature of viscosities at a shear rate of 275 s^{-1} at the die lip of sheet-extrusion T-die. Compared at an equivalent MFI, to make the viscosity of MET-PP equivalent to that of ZN-PP, the extrusion temperature of the former should be raised by 30–40°C.

Figure 7 shows the dependence of viscosity at sheet extrusion on MFI. To make the viscosity of MET-PP equivalent to that of ZN-PP, MFI should to be raised 2–2.5 times.

Figure 8 shows temperature changes of viscosities at various shear rates (Arrhenius plots) for the MET-1 sample as an example. The flow activation energies ΔHa obtained from the slopes of the lines are shown at the right side of the figure. ΔHa decreases with increasing shear rate.

Figure 9 shows the changes of flow activation energies ΔHa with shear rate. Although MET-PPs tend to show higher ΔHa than ZN-PPs at low shear rates (<100 s^{-1}), they inversely tend to show lower ΔHa at high shear rates (>100 s^{-1}).

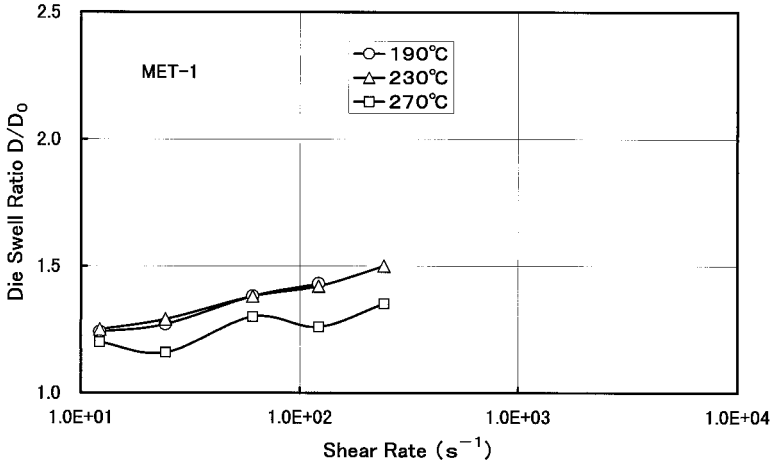

Figure 10 Changes of die–swell ratios D/D_0 of MET-1 sample at various temperatures with shear rate.

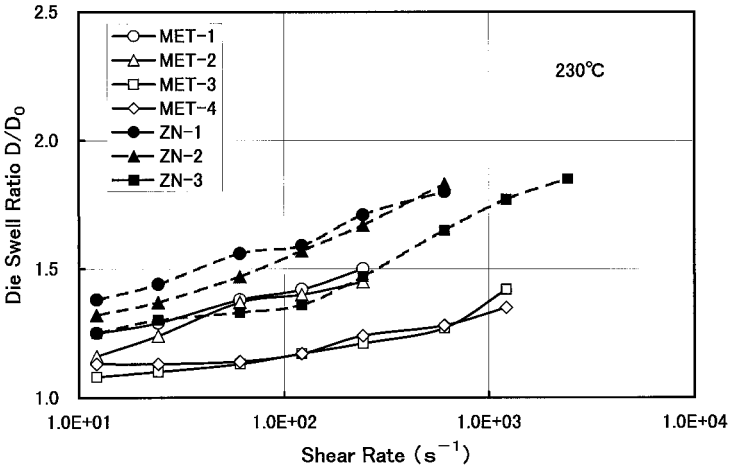

Figure 11 Comparison of change of die–swell ratio D/D_0 with shear rate among samples at 230°C.

Accordingly, it may be said that MET-PPs show low temperature changes of viscosity at high shear rates of extrusion and injection molding and hence have superior processing stabilities there.

Die Swell

Figure 10 shows the changes with shear rate of die swell ratio D/D_0 at various temperatures for MET-1 sample as an example. The die–swell ratio tends to increase with decreasing temperature and with increasing shear rate.

Figure 11 shows the comparison among samples of the change of die swell ratio with shear rate at 230°C as an example. The die–swell ratio is higher as the MFI is lower and compared at an equivalent MFI, MET-PPs with narrower molecular weight distributions show lower die swell ratios than ZN-PPs.

The die–swell ratio at a constant shear rate is generally higher as the molecular weight is higher and the molecular weight distribution is broader. The effect of molecular weight is reported for PP,[5,6] polyethylene (PE),[7,8] high-density polyethylene (HDPE),[9] and polychloroprene.[10,11] The effect of molecular weight distribution is reported for PP in relation to general molecular weight distribution[12] and in relation to M_w/M_n and M_z/M_w,[6] for PE in relation to M_w/M_n,[8]

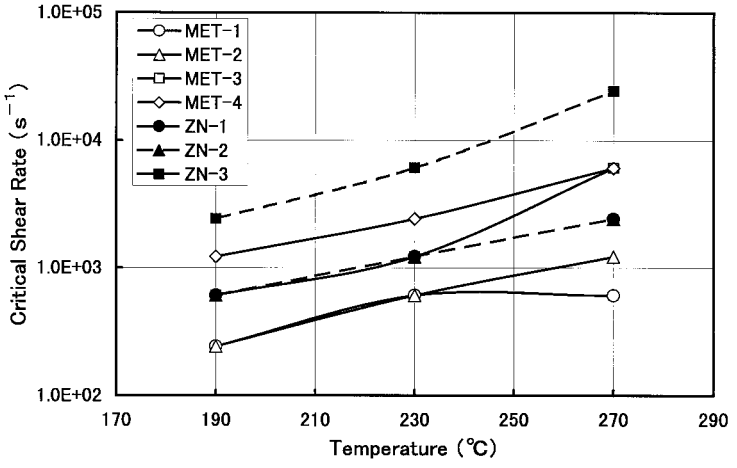

Figure 12 Temperature changes of critical shear rates at which melt fractures begin to occur.

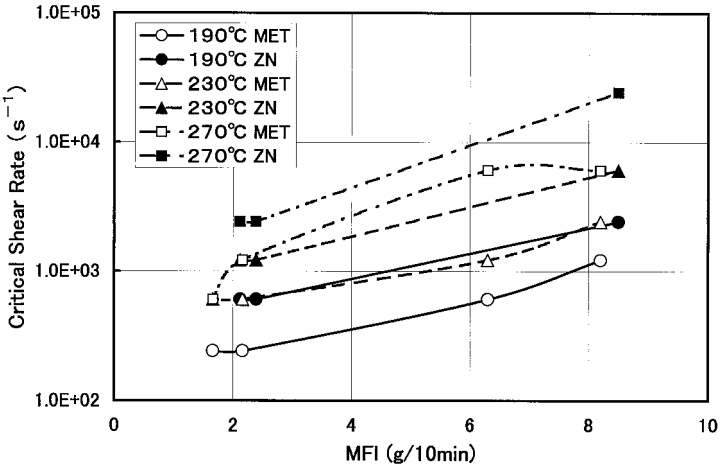

Figure 13 MFI dependences of critical shear rates at which melt fractures begin to occur.

for HDPE in relation to M_w/M_n,[9] and for polychloroprene in relation to M_z/M_w.[10] It may be said that MET-PPs show a similar dependence of die–swell behavior on the molecular weight and its distribution to that of general thermoplastic resins.

Melt Fracture

Figure 12 shows the temperature changes of critical shear rates at which gross melt fractures begin to occur. The critical shear rate increases with increasing temperature. Compared at an equivalent MFI, MET-PPs show lower critical shear rates than ZN-PPs and to make the critical shear rate of MET-PP equivalent to that of ZN-PP, the extrusion temperature of the former should be raised by about 40°C.

Figure 13 shows the dependence of critical shear rate on MFI. It increases with MFI and to make the critical shear rate of MET-PP equivalent to that of ZN-PP, the MFI should be raised two to three times.

The increase of critical shear rate $\dot{\gamma}_c$ with increasing MFI or with decreasing molecular weight is also generally reported for PP[6,12,13] and other polymers.[11,14–21] As for the effect of molecular weight distribution, Fujiyama et al.[6] found that $\dot{\gamma}_c$ increases with increasing M_z/M_w and is

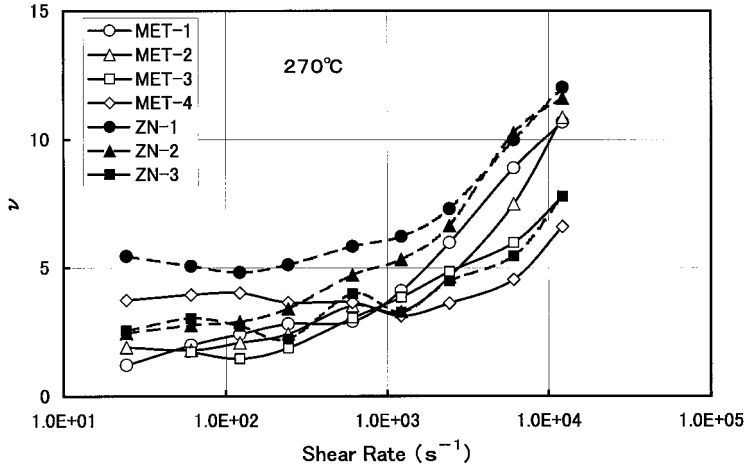

Figure 14 Comparison of change of end correction coefficient ν with shear rate among samples.

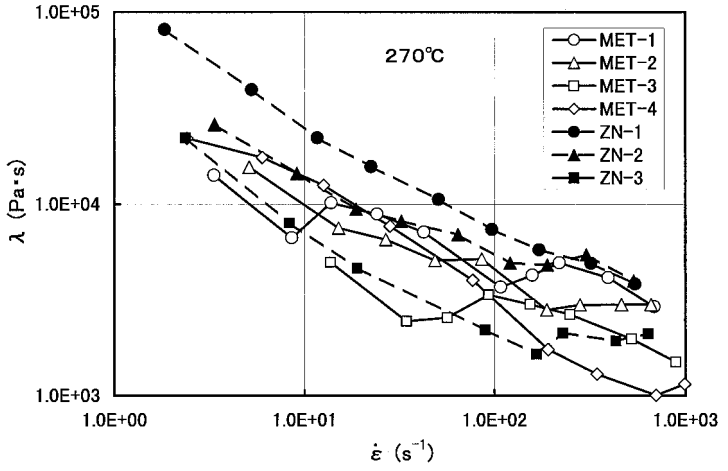

Figure 15 Comparison of change of elongational viscosity λ with elongational strain rate $\dot{\epsilon}$ among samples.

proportional to M_z/M_w^2. Stabler et al.[22] found that $\dot{\gamma}_c$ of HDPE is higher as the molecular weight distribution is broader. Goyal et al.[23] report that $\dot{\gamma}_c$ of LLDPE increases with increasing molecular weight distribution M_w/M_n below 10 and steeply drops at M_w/M_n above 10. The experimental results of $\dot{\gamma}_c$'s for MET-PPs and ZN-PPs in the present study are generally on the same line of these previous findings in the sense of dependence on molecular weight and its distribution.

End Correction Coefficient, Elongational Viscosity, and Melt Tension

Figure 14 shows the comparison among samples of change of end correction coefficient ν with shear rate. ν increases with decreasing MFI and with increasing shear rate. Compared at an equivalent MFI, MET-PPs show lower ν than ZN-PPs. Low ν causes a low pressure loss at the part where the shape of cross section of flow path changes.

The fact that ν is higher as the MFI is lower or the molecular weight is higher is generally reported for PP[6,12,13,24–26] and other polymers.[10,15,16,27–29] The fact that comparing at an equivalent MFI (molecular weight), ν is higher as the molecular weight distribution is broader is reported for PP by Kamide and Fujii,[24] Fujiyama and Awaya,[21] and Fujiyama et al.,[6] for HDPE by LaMantia et al.,[30] and for chloroprene by Kawasaki et al.[10,16] The experimental results for ν's of MET-PPs and ZN-PPs can be explained from the viewpoint of the difference in molecular weight distribution.

Figure 15 shows the comparison among samples of change of elongational viscosity λ with elongational strain rate $\dot{\epsilon}$. λ decreases with increasing MFI and $\dot{\epsilon}$. Compared with an equivalent MFI, MET-PPs show lowerλ's than ZN-PPs.

Figure 16 shows the relation between melt tension MT and MFI. MT and MFI show an negative correlation on log–log plot. Compared at an equivalent MFI, MET-PPs show lower MTs than ZN-PPs. To make the MT of MET-PP equivalent to that of ZN-PP, the temperature should be lowered by about 40°C.

Mori and Saito[31] show that compared at an equivalent MFI, MET-PPs show lower MTs than ZN-PPs as in the present experimental results. Ghijsels and De Clippeleir[32] show that the controlled-rheology PP series, which were prepared

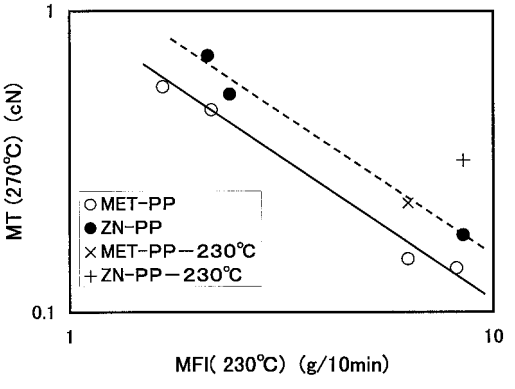

Figure 16 Relation between melt tension MT and melt flow index MFI.

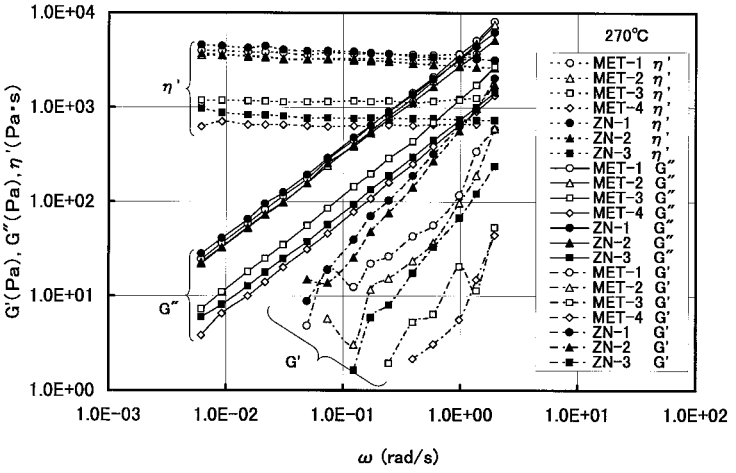

Figure 17 Comparison of storage modulus G', loss modulus G'', and dynamic viscosity η' among samples.

by degrading reactor-type ZN-PPs with a peroxide, and decreased in molecular weight and its distribution show lower MTs than the original reactor-type ZN-PP series compared at an equivalent MFI. They also show that when MTs are plotted against zero-shear viscosities η_0's, both PP series ride on the same straight line. From above, the fact that MT of MET-PP is lower than that of ZN-PP compared at an equivalent MFI is assumed to be because compared at an equivalent MFI, the zero-shear viscosity η_0 of the former is lower than that of the latter because of the narrower molecular weight distribution of the former, as shown later in Figure 18.

Because of their low elongational viscosity and melt tension, MET-PPs are assumed to show superior melt extensibility at spinning or film extrusion and are able to be spun or extruded at high speed without draw resonance. It is assumed to be particularly suitable to extrusion lamination. Actually, Cheng and Kuo[4] show that an MET-PP can be cast by T-die without draw resonance up to a haul-off speed 17% higher than that of a ZN-PP with an equivalent MFI to that of the MET-PP.

Dynamic Viscoelasticity

Figure 17 shows the comparison of dynamic viscoelasticities among samples. Compared at an equivalent MFI, although the viscosity expressed by the dynamic viscosity η' and the loss modulus G'' is similar for MET-PPs and ZN-PPs, the elas-

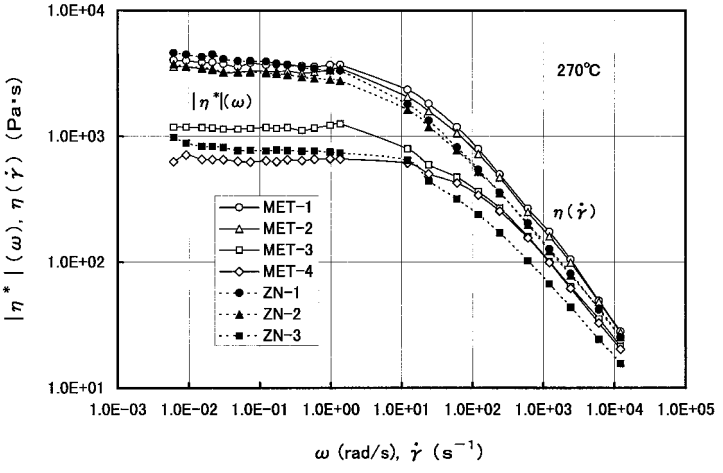

Figure 18 Comparison of flow curve among samples.

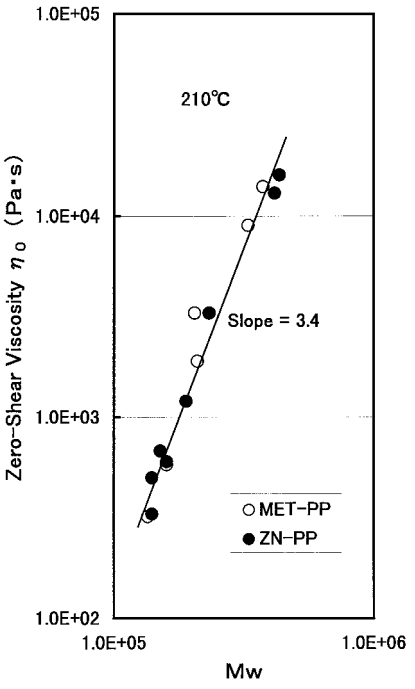

Figure 19 Relation between zero-shear viscosity η_0 and weight-average molecular weight M_w.

ticity expressed by the storage modulus G' is very (about one decade) lower for the former than for the latter, which means that the relaxation time is shorter and the elasticity is weaker for the former.

Figure 18 shows flow curves in a wide shear rate range, which were obtained as the absolute values of complex viscosities $|\eta^*|(\omega)$ from dynamic viscoelastities and as the steady-state viscosities $\eta(\dot{\gamma})$ from capillary flow properties. That the absolute value of complex viscosity $|\eta^*|(\omega)$ and the steady-state viscosity $\eta(\dot{\gamma})$ are equivalent functions is known as the Cox–Merz's empirical law[33] and is widely applied to evaluate the flow properties of polymer melts. Comparing the viscosity of MET-PP with that of ZN-PP at an equivalent MFI, the former is lower than the latter at low shear rates, whereas the former is higher at high shear rates. From this it may be said that MET-PP is inferior in shape-holding ability in the molten state and is easy to cause drawdown. Furthermore, it is also inferior in fluidity at extrusion and injection molding where high shear rates are encountered.

The fact that comparing the viscosity of MET-PP with that of ZN-PP the former is lower at low shear rates while the former is higher at high shear rates has been already reported.[4,31,34]

Figure 19 shows a log–log plot of the zero-shear viscosity η_0 (viscosity at extreme low shear rate in Fig. 18) against the weight-average molecular weight M_w. Regardless of the kind of catalyst, the relation is expressed by a straight line with a slope of 3.4 and the well-known 3.4th-power law[35] holds.

Evaluation as Raw Resin for Sheet-Extrusion

When MET-1 sample (MFI = 1.66 g/10 min) and MET-2 sample (MFI = 2.16 g/10 min) out of MET-PPs in the present experiment were sheet-extruded with an extruder equipped with a T-die at a resin temperature of 270°C, the extrusion torque rose too much and a gross melt fracture occurred under the usual extrusion conditions. Accordingly, to obtain high-quality sheet, the ex-

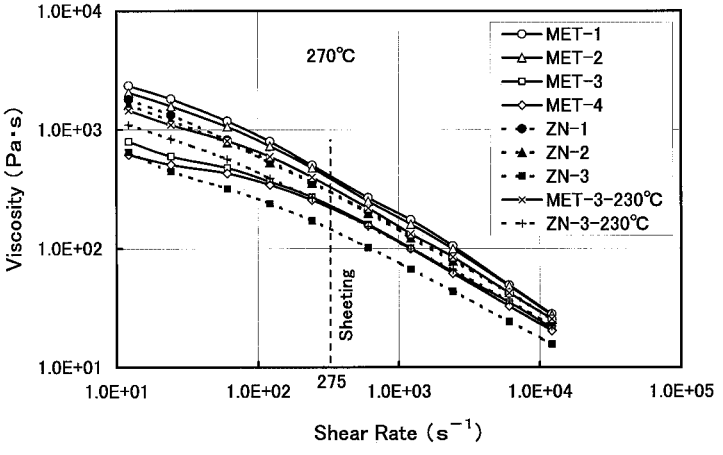

Figure 20 Comparison of flow curve among samples.

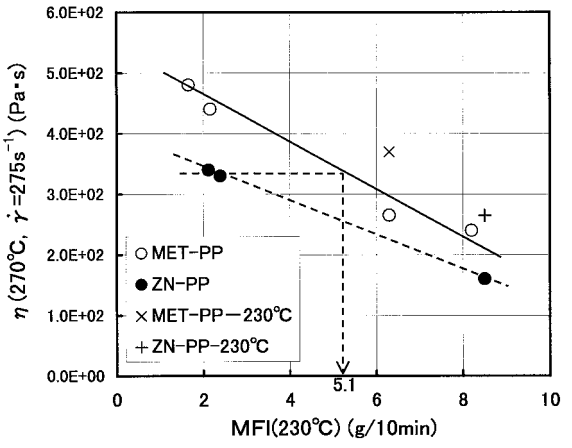

Figure 21 Relation between viscosity at sheeting and MFI.

trusion must be operated at a low line speed and the productivity rate was very low. Then, the selection of proper MFI and extrusion temperature was studied by means of rheological measurements.

Figure 20 shows the comparison of flow curve among samples. As shown by a vertical broken line in the figure, the shear rate at the die lip under usual sheet-extrusion conditions is 275 s^{-1}. At this shear rate, the viscosity of the MET-3 sample (MFI = 6.3 g/10 min) at 230°C is equivalent to those of ZN-1 sample (MFI = 2.1 g/10 min) and ZN-2 sample (MFI = 2.5 g/10 min), which are ZN-PPs for sheet extrusion, at 270°C (usual sheet-extrusion temperature).

Figure 21 shows the relation between the viscosity at sheet extrusion and MFI. Compared at an equivalent MFI, MET-PPs show higher viscosities than ZN-PPs. It is seen in this figure that to make the viscosity of MET-PP equivalent to those of ZN-PPs for sheet extrusion, the MFI of MET-PP may be set to about 5 g/10 min. Under this estimation, MET-3 (MFI = 6.3 g/10 min) was used. Because the MFI of this sample is slightly higher than the estimated value, the sheet extrusion was performed at 230°C, resulting in fine extrusion without torque rise and melt fracture. The viscosity value at 230°C of MET-3 is shown by a mark × in Figure 21, which is only slightly higher than those of ZN-PPs for sheet extrusion at 270°C. The viscosity value of the ZN-3 sample at 230°C is also shown in Figure 21, which rides on the straight line, showing the relation for MET-PPs at 270°C.

Figure 22 shows the relation between the critical shear rate at which a melt fracture begins to occur and MFI. In this figure, the lower limit shows the shear rate at which a melt fracture still does not occur and the upper limit shows the shear rate at which a melt fracture already occurs. From this figure, to make the melt fracture behaviors of MET-PP equivalent to those of ZN-PPs for sheet extrusion, the MFI of MET-PP may be set to about 3.6 g/10 min. Actually, the MET-3 sample with an MFI of 6.3 g/10 min was used, whose critical shear rate at 230°C (×) is equivalent to those of ZN-PPs for sheet extrusion at 270°C (●). In fact, when the MET-3 sample was

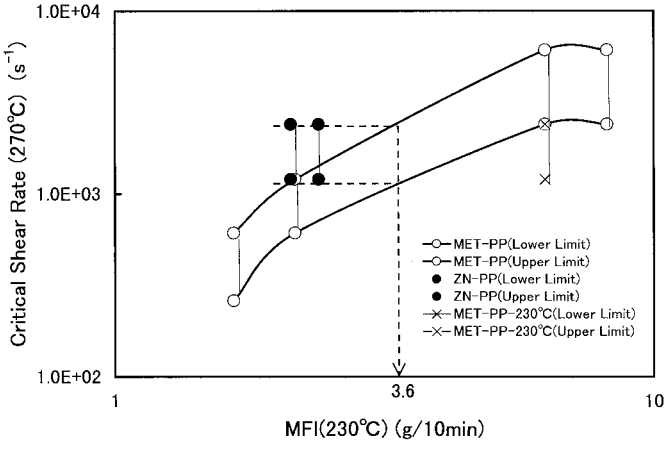

Figure 22 Relation between critical shear rate at which melt fracture begins to occur and MFI.

Table II Rheological Characteristics of Metallocene PP (Compared with Ziegler-Natta PP at Equivalent MFI)

Characteristics of Rheological Properties	Influence on Processibilities and Higher Order Structures
Viscosity at low shear rates is low and viscosity at high shear rates is high.	Drawdown is large and not suitable to blow molding and thermoforming. Fluidity is low at extrusion and injection molding.
Although loss modulus G'' (viscosity) scarcely differs, storage modulus G' (elasticity) is very (about one decade) low.	Because elasticity is low and relaxation time is short, suitable to fields where low resilience is needed. Molecular orientation of processed article is low, surface smoothness is high and suitable to precision molding.
Die swell is very small.	Suitable to profile extrusion (low MFI is needed).
Entrance pressure loss and end correction coefficient are low.	Pressure loss at part where shape of cross section of flow path changes at extrusion is low.
Critical shear rate at which melt fracture begins to occur is low.	Melt fracture is easy to occur at extrusion.
Melt tension and MFIR are low.	High-speed drawability is good and suitable to T-die extrusion, extrusion lamination, inflation extrusion, and spinning. However, neck-in is large.
Elongational viscosity is low.	Drawdown is large.
Relation between zero-shear viscosity and weight-average molecular weight obeys 3.4-th power law.	
Flow activation energy is a little low.	Processing stability is good.

sheet-extruded at 230°C, it could be processed without problems such as melt fracture under usual line speed.

CONCLUSION

Table II lists the rheological characteristics of MET-PPs obtained from the present experiments and estimations of their influence on melt processibilities and higher order structures. The present study made clear the rheological characteristics of MET-PPs and offered data for the free selection and setting of MFI of raw resin and processing conditions in various processes of the PPs. Namely, as an example for sheet extrusion, to make the viscosity of MET-PP equivalent to that of ZN-PP, the MFI of the former may be raised by 2–2.5 times or the temperature may be elevated by 30–40°C. To make the melt fracture behaviors of MET-PP equivalent to those of ZN-PP, the MFI of the former may be raised by about three times or the temperature may be elevated by about 40°C.

The authors thank Tokuyama Corp. for permission to publish this article.

REFERENCES

1. Sinn, H.; Kaminsky, W. Adv Organomet Chem 1980, 18, 99.
2. Sinn, H.; Kaminsky, W.; Vollmer, H.; Waldt, R. Angew Chem, Int Ed Engl 1980, 19, 390.
3. Cogswell, F. N. Polym Eng Sci 1972, 12, 64.
4. Cheng, C. Y.; Kuo, J. W. C. J Plast Film Sheet 1999, 15, 82.
5. Kamide, K.; Inamoto, Y.; Ohno, K. Kobunshi Kagaku 1965, 22, 529.
6. Fujiyama, M.; Kitajima, Y.; Inata, H. J Appl Polym Sci 2002, 84, 2128.
7. Beynon, D. L. T.; Glyde, B. S. Br Plast 1960, 33, 414.
8. Rogers, M. G. J Appl Polym Sci 1970, 14, 1679.
9. Fleissner, Von M. Angew Makromol Chem 1973, 33, 75.

10. Kawasaki, N.; Ohno, S. Kobunshi Ronbunshu 1974, 31, 1.
11. Kawasaki, N.; Yamagata, Y.; Ohno, S.; Hahsimoto, T. Nihon Gomu Kyokaishi 1973, 16, 502.
12. Fujiyama, M.; Awaya, H. J Appl Polym Sci 1972, 16, 275.
13. Fujiyama, M.; Kagiyama, Y. Kobunshi Kagaku 1972, 29, 191.
14. Fukazawa, Y. Kogyo Kagaku Zasshi 1960, 63, 459.
15. Fujiyama, M.; Wakino, T. Nihon Reoroji Gakkaishi 1991, 19, 64.
16. Kawasaki, N.; Ohno, S.; Fukuda, M. Kobunshi Kagaku 1973, 30, 485.
17. Spencer, R. S.; Dillon, R. E. J Colloid Sci 1949, 4, 241.
18. Mills, D. R.; Moore, G. E.; Pugh, D. W. SPE Trans 1961, 1, 40.
19. Bagley, E. B. Trans Soc Rheol 1961, 5, 355.
20. Doring, G.; Leusering, H. J. Kunststoffe 1963, 53, 11.
21. Sieglaff, C. L. SPE Trans 1964, 4, 459.
22. Stabler, H. G.; Haward, R. N.; Wright, B. Advances in Polymer Science and Technology; S. C. I. Monograph, No.6, 1967, p 327.
23. Goyal, S. K.; Kazatchkov, I. B.; Bohnet, N.; Hatzikiriakos, S. G. SPE Tech. Paper; 55th ANTEC; 1997, 43, 1076.
24. Kamide, K.; Fujii, K. Kobunshi Kagaku 1967, 24, 120.
25. Grant, D. E.; Dieckmann, S. F. J Appl Polym Sci 1965, 9, 3231.
26. Tzoganakis, C.; Vlachopoulos, J.; Hamielec, A. E. Polym Eng Sci 1989, 29, 390.
27. Ram, A.; Narkis, M. J Appl Polym Sci 1966, 10, 361.
28. Kataoka, T.; Ueda, S. J Appl Polym Sci 1968, 12, 939.
29. Arai, T.; Aoyama, H. Trans Soc Rheol1963, 7, 333.
30. LaMantia, F. P.; Valenza, A.; Acierno, D. Rheol Acta 1983, 22, 299.
31. Mori, K.; Saito, J. Seikei-Kakou 1996, 8, 649.
32. Ghijsels, A.; De Clippeleir, J. Int Polym Process 1994, 9, 3.
33. Cox. W. P.; Merz, E. H. J Polym Sci 1958, 28, 619.
34. Cheng, C. Y. SPE Tech. Paper; 54th ANTEC; 1996, 42, 2019.
35. Bueche, F. J Chem Phys 1956, 25, 599.